Diamond-Modified AFM Probes: From Diamond Nanowires to Atomic Force Microscopy-Integrated Boron-Doped Diamond Electrodes

ARTICLE *in* ANALYTICAL CHEMISTRY · JUNE 2011

Impact Factor: 5.64 · DOI: 10.1021/ac200659e · Source: PubMed

analytical chemistry

ARTICLE

pubs.acs.org/ac

Diamond-Modified AFM Probes: From Diamond Nanowires to Atomic Force Microscopy-Integrated Boron-Doped Diamond Electrodes

Waldemar Smirnov,*[,†] Armin Kriele,[†] René Hoffmann,[†] Eugenio Sillero,[‡] Jakob Hees,[†] Oliver A. Williams,[†,∥] Nianjun Yang,[†] Christine Kranz,[§] and Christoph E. Nebel[†]

[†]Fraunhofer Institut für Angewandte Festkörperphysik, Tullastrasse 72, Freiburg 79108, Germany

[‡]ISOM-DIE, Universidad Politécnica de Madrid, 28040 Madrid, Spain

[§]Institute of Analytical and Bioanalytical Chemistry, University of Ulm, Albert-Einstein-Allee 11, 89081 Ulm, Germany

Supporting Information

ABSTRACT: In atomic force microscopy (AFM), sharp and wear-resistant tips are a critical issue. Regarding scanning electrochemical microscopy (SECM), electrodes are required to be mechanically and chemically stable. Diamond is the perfect candidate for both AFM probes as well as for electrode materials if doped, due to diamond's unrivaled mechanical, chemical, and electrochemical properties. In this study, standard AFM tips were overgrown with typically 300 nm thick nanocrystalline diamond (NCD) layers and modified to obtain ultra sharp diamond nanowire-based AFM probes and probes that were used for combined AFM−SECM measurements based on integrated boron-doped conductive diamond electrodes. Analysis of the resonance properties of the diamond overgrown AFM cantilevers showed increasing resonance frequencies with increasing diamond coating thicknesses (i.e., from 160 to 260 kHz). The measured data were compared to performed simulations and show excellent correlation. A strong enhancement of the quality factor upon overgrowth was also observed (120 to 710). AFM tips with integrated diamond nanowires are shown to have apex radii as small as 5 nm and where fabricated by selectively etching diamond in a plasma etching process using self-organized metal nanomasks. These scanning tips showed superior imaging performance as compared to standard Si-tips or commercially available diamond-coated tips. The high imaging resolution and low tip wear are demonstrated using tapping and contact mode AFM measurements by imaging ultra hard substrates and DNA. Furthermore, AFM probes were coated with conductive boron-doped and insulating diamond layers to achieve bifunctional AFM−SECM probes. For this, focused ion beam (FIB) technology was used to expose the boron-doped diamond as a recessed electrode near the apex of the scanning tip. Such a modified probe was used to perform proof-of-concept AFM−SECM measurements. The results show that high-quality diamond probes can be fabricated, which are suitable for probing, manipulating, sculpting, and sensing at single digit nanoscale.

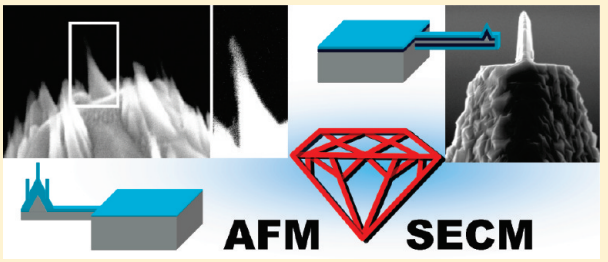

The development of new analytical methods for providing information on biological systems and their molecular interactions is an emerging field in modern life sciences. Among the scanning probe microscopy (SPM) techniques, which are key to this emerging field, atomic force microscopy (AFM) is the most versatile and widespread representative, which may not only be applied in air, but also in liquid, allowing imaging biological entities in buffered solutions. Among the ongoing pertinent research topics are approaches improving the physical properties of AFM cantilevers such as their Q factors for stable imaging in solution, and adding chemical functionality to the imaging probe. One approach here is the chemical functionalization of AFM probes, which allows detecting and quantifying forces associated with single molecule binding events at ambient conditions. Within the past decade, combining complementary scanning probe techniques such as combination of AFM with scanning near-field optical microscopy (NSOM)[1] or combining NSOM with scanning ion conductance microscopy (SICM) have emerged.[2,3] Apart from those techniques, scanning electrochemical microscopy (SECM) provides localized information on interfacial and biological processes on challenging subjects such as cellular signaling at molecular level. This scanning probe technique is sensitive to the nature of the substrate and the presence of electroactive species[4,5] and has been proven to be a valuable technique for the characterization of chemical surface properties with high spatial resolution. For example, progress in cell biological and bioanalytical science,[6−10] chemistry,[11,12] or issues related to energy[13] reveals the interdisciplinary research areas of SECM. Of particular interest is the powerful combination of AFM and SECM[14,15] to simultaneously obtain unique and correlated topographical and electrochemical properties of a specimen.[16−18] Several fabrication schemes of such AFM−SECM

Received: March 15, 2011
Accepted: May 2, 2011
Published: May 02, 2011

probes have been developed focusing on a design with the electroactive area at the apex of the AFM tip[14,19−22] or with an electrode recessed from the tip apex.[16,23,24]

The development of sharp and wear-resistant SPM probes is an important issue, because they are nowadays routinely used in nearly all fields of science. Sharp tips have been developed for probing, manipulating, machining, and fabricating at the nanoscale. AFM related nanolithographic techniques are used for three-dimensional mechanical patterning of resists,[25] the modification of local surface chemistry,[26,27] dip-pen nanolithography,[28] or direct and precise delivery of biomolecules,[29] to name a few. These techniques have also been used for nanoelectronics[30] and data storage.[31] An enhanced resolution was shown to be achieved by mounting[32,33] or by growth[34,35] of sharp objects such as carbon nanotubes on commercial AFM tips.

However, most manufactured tips are either sharp but not wear-resistant or mechanically strong but blunt. With respect to integrating functionality to scanning probe techniques as demonstrated by a combination of AFM and SECM, the physical and chemical properties of the integrated electrode material are an important concern in particular regarding biological relevant applications. The electrode should retain its integrity after extended use in air, water, and harsh environments. Usually metals such as gold and platinum are used as electrode materials in combined AFM−SECM probes. However, noble metal electrodes show some disadvantages, for example, limited potential window and electrode fouling in particular when applied in complex biological matrices. Hence, materials, which show high mechanical stability as well as good electrochemical properties, are ideal for combined SPM probes. Among such materials are diamond and boron-doped diamond, which are the perfect candidates for AFM probes as well as electrode materials. Diamond is exceptionally hard, stable, and wear-resistant due to its high Young's modulus of 1220 GPa[36] in comparison to much lower values of silicon (185 GPa) or silicon nitride (250 GPa). Furthermore, it is chemically inert, can be deposited with tailored conductive properties ranging from insulating to metallic-like conductance, and has outstanding electrochemical properties, such as a wide electrochemical potential window and very low background currents.[37] These properties make diamond ideal for surface probing and electrochemical sensing applications.[38]

Typically, commercially available diamond AFM probes are fabricated by overgrowth of silicon tips using plasma-enhanced chemical vapor deposition (CVD),[39] hot filament-assisted CVD,[40] or by growth of diamond into a silicon mold.[39,41−45] The wear resistance of ultrananocrystalline diamond (UNCD)-coated tips increases at least 1 order of magnitude as compared to silicon nitride tips.[46,47] However, tips coated with very small diamond crystals may suffer from abrupt fracture and detachment of clusters.[45,48] Therefore, coating probes uniformly with diamond of higher quality is important, which in turn has drawbacks considering image resolution due to larger diamond crystals and higher surface roughness.

RESULTS AND DISCUSSION

In this Article, a fabrication method allowing the formation of sharp diamond nanowhiskers at the apex of a diamond-coated AFM probe, serving as ultra sharp diamond AFM tip, is presented. With the same process, boron-doped diamond electrodes integrated in AFM probes for combined AFM−SECM measurements can be processed. The approach is based on CVD diamond coating of silicon cantilevers and on diamond nanowire technology.[49]

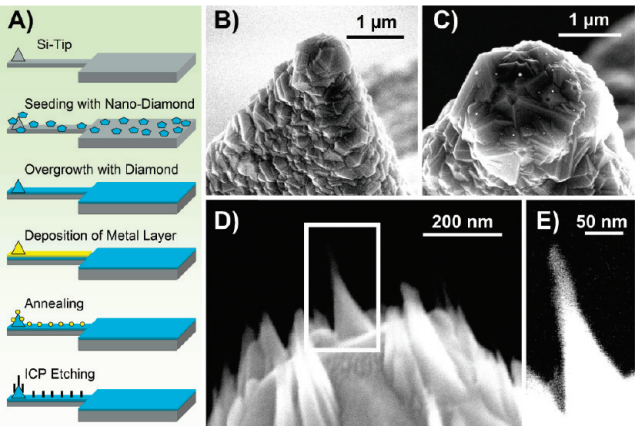

Figure 1. (A) A schematic of the fabrication process: from diamond deposition to sharpening of the tip. (B) SEM image of a diamond-coated silicon AFM tip. (C) SEM image of self-organized gold nanomask at the tip apex. (D) SEM image of etched diamond nanowires at the tip apex. (E) Magnified SEM image of one single nanowire.

Briefly, standard silicon AFM tips were coated with electrically conducting (boron-doped) and insulating nanocrystalline diamond (NCD) layers. The obtained tips with a significantly increased tip radius were then sharpened by a plasma etching process using self-organized metal nanomasks. After etching, apex radii as small as 5 nm could be obtained. On the basis of this effective method, high-quality diamond probes can be fabricated suitable for probing, manipulating, sculpting, and sensing at single digit nanoscale. A thorough characterization of these probes with respect to their resonance frequency and the quality factor is shown. The improved AFM imaging quality and wear resistance is demonstrated by imaging ultra hard substrates and DNA. Moreover, such diamond-coated AFM probes can be transformed into bifunctional probes by exposing the boron-doped diamond as recessed electrode using FIB technology, which was used to perform a proof-of-concept AFM−SECM measurement.

Fabrication. Figure 1A shows a schematic of the fabrication steps including the seeding of commercial silicon tips with nanodiamond particles from a colloidal solution[50−52] prior to the subsequent overgrowth of these tips with nanocrystalline diamond using plasma-enhanced CVD. With increasing diamond thickness, the tip radii become rough and require sharpening to allow high-resolution AFM imaging. To achieve this, self-organized metal nanomasks were used in a plasma etching process. To generate these masks, a thin gold layer is deposited on the cantilevers and is thermally annealed in an induction furnace. Because of the melting point lowering of thin metal layers in comparison to their corresponding bulk materials, the gold layer begins to melt at temperatures as low as 700 °C.[53] Because of surface energy differences between metal and substrate surface, self-organized gold particles can be formed.[54] The nanoparticles are used as nanomasks in a ICP reactive ion etching process, which etches the unmasked diamond substrate and results in diamond nanowires at the AFM tips. To achieve optimal mask conditions with small gold particles with optimized interparticle spacing, the gold layer thickness, annealing temperature, and

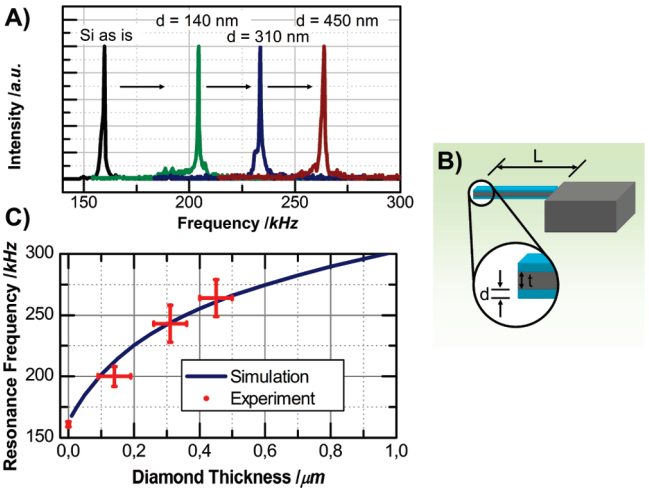

Figure 2. (A) Resonance frequency of cantilevers with different thicknesses of the diamond coating. (B) Schematic of cantilever coated with diamond. (C) Comparison of measured resonance frequency with simulated values using Ansys.

annealing duration have to be carefully controlled. Large spacing between the gold particles will guarantee optimal-spaced nanowires avoiding multiple wires at the tip apex and thus minimizing imaging artifacts as only one nanowire creates the topography image. The length and thus aspect ratio of the diamond wires can be adjusted by the etching duration. It should be noted that nanostructures such as nanowires exhibit ultrastrength phenomena as compared to their bulk material properties,[55,56] which is of particular advantage regarding applications as scanning probes.

Scanning electron microscopy (SEM) images of diamond overgrown silicon tips that were subsequently sharpened are shown in Figure 1B− E. Figure 1B reveals a tip with a 350 nm thick diamond coating. It is evident that the tip radius is about 450 nm. In Figure 1C, gold nanomasks are clearly visible as small bright dots. Their size is measured to be 40 ± 10 nm. Figure 1D shows a plasma-etched tip. A magnification of the nanowire at the tip apex with a radius of 5 nm is shown in Figure 1E.

Resonance Behavior. The resonance properties of the overgrown cantilevers were analyzed using a vibrometer and a standard AFM setup with a piezo-actuator and a laser. Figure 2A shows the resonance frequency shift of the overgrown cantilevers, depending on the diamond film thickness.

With increasing thickness of the deposited diamond layer deposited on the silicon cantilevers, the resulting resonance frequency increases, which is related to diamond's high Young's modulus. Regarding eq 1 of a single-side clamped cantilever, it is evident that the resonance frequency f_0 increases with increasing Young's modulus E and the thickness of the cantilever t:

$$f_0 = \frac{t}{2\pi L^2}\sqrt{\frac{E}{\rho}} \qquad (1)$$

where L is the cantilever length and ρ is the density of the cantilever material (Figure 2B). This is only valid, however, if the resonator consists of one material. In our case, the cantilever is composed of Si wrapped by a diamond coating with varying thickness. Different models have been proposed for the characterization of the dynamic behavior of such multilayer cantilevers. Nevertheless, these models use approximations that disregard surface effects, which may have a strong impact for such thin layers applied for coating the cantilevers. Therefore, a 3D finite element numerical model (FEM) was derived using ANSYS software. The FEM analysis takes the geometry of the cantilever, the densities, and the Young's moduli of silicon and diamond into consideration. The simulated resonance frequency dependence of the diamond layer thickness is compared to the measured resonance frequencies of the samples shown in Figure 2C. The error bars relate to the standard deviations of five overgrown cantilevers having nominally the same diamond thickness. A comparison of overgrown cantilevers with the simulated data shows a good agreement. The obtained data reveal that a defined resonance frequency can be adjusted by choosing a defined diamond coating thickness. Moreover, peak-shape analysis of the resonance frequencies before and after overgrowth shows an enhancement in the quality factor, which is defined by $Q = f/w$, where f denotes the resonance frequency and w is the full-width at half-maximum (FWHM) of the resonance peak. A silicon cantilever with resonance frequency of f_{Si} = 130 kHz and a quality factor of Q_{Si} = 120 increased by coating with 850 nm diamond to f_{coated} = 370 kHz and to Q_{coated} = 710, which corresponds to an increase of +185% and +490%, respectively. The enhancement in Q-factor is higher than expected and may be attributed to the uniform diamond coating, which is hermetically wrapped around the silicon cantilever, resulting in a strong and rigid structure. It also proves that the interface between silicon and diamond is of high quality because no dissipative effects are occurring. The real time visualization of the first- and second-order oscillation of diamond-coated cantilevers was obtained with a vibrometer setup and can be seen in the Supporting Information.

AFM Scanning Performance. The overgrown and sharpened nanowire tips were tested with respect to their imaging quality in tapping and contact mode, respectively. The achieved resolutions as well as the wear properties were investigated and show superior characteristics as compared to (A) commercially available silicon and (B) commercially available diamond AFM probes as indicated in Figure 3. As a measure of resolution, single-stranded λ-phage DNA on mica was imaged in tapping mode (Figure 3 A1−C1 and A2−C2). Analyzing cross sections of the DNA images (Figure 3D), the tip radius can be obtained. The real width of the DNA is assumed to be in the order of 1 nm. The measured width of the DNA, however, is a convolution of the scanning tip geometry and the actual DNA width. Taking this into consideration, similar tip radii of (7−9) nm for both the standard silicon tip and our diamond nanowire probes were obtained. It should be noted that the DNA structures cannot be resolved using a commercially available diamond-coated AFM tip.

Measurements regarding the wear characteristics were carried out by imaging an ultra hard and rough substrate, in this case, a nanocrystalline diamond surface. For direct comparison, the scanned area was selected to be the same spot of the imaged substrate for different probes. A tapping mode scan is shown in Figure 3A3−C3. The resolution of the standard silicon tip (Figure 3A3) is comparable to that of our sharpened tip (Figure 3C3), while the commercial diamond-coated tip (Figure 3B3) was found to be inferior in performance. When imaging the hard model sample in contact mode, the imaging quality obtained with the silicon tip deteriorated within the first recorded scan (Figure 3A4) due to abrasion of the tip. While the commercial diamond tip suffered from fracture during the first three scans in contact mode (Figure 3B4), our nanowire tip

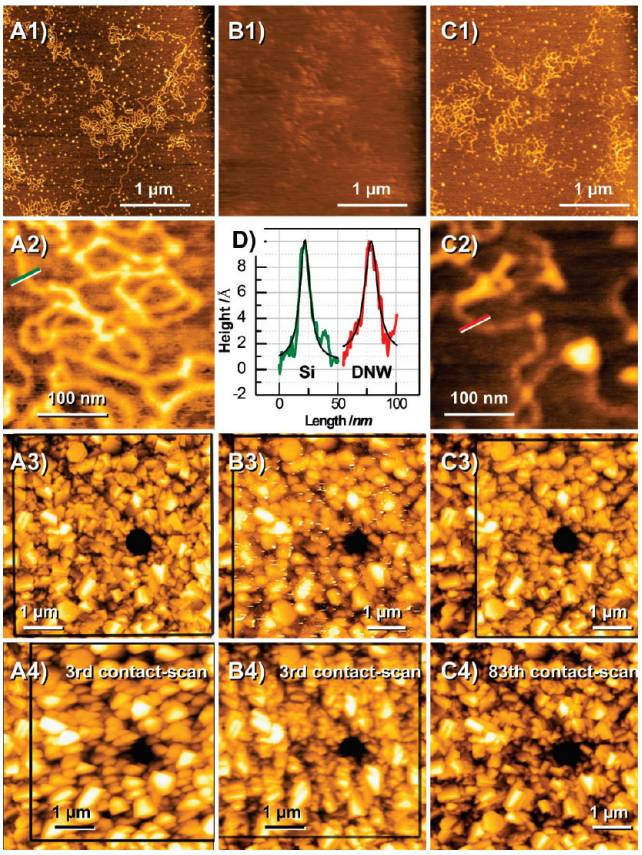

Figure 3. AFM images showing wear and resolution characteristics of a standard silicon probe (A), of a commercial diamond tip (B), and of our sharpened diamond tip (C). Shown are tapping mode scans of λ-phage DNA on mica (2) and a higher magnification image (3). Tapping mode and contact mode AFM scans on the same spot of a nanocrystalline diamond sample are shown in (3) and (4), respectively. (D) Line scan and Lorentz fits of Si-tip and diamond nanowire tip (DNW) denoted in (A2) and (C2) as green and red lines, respectively. Images were recorded in air.

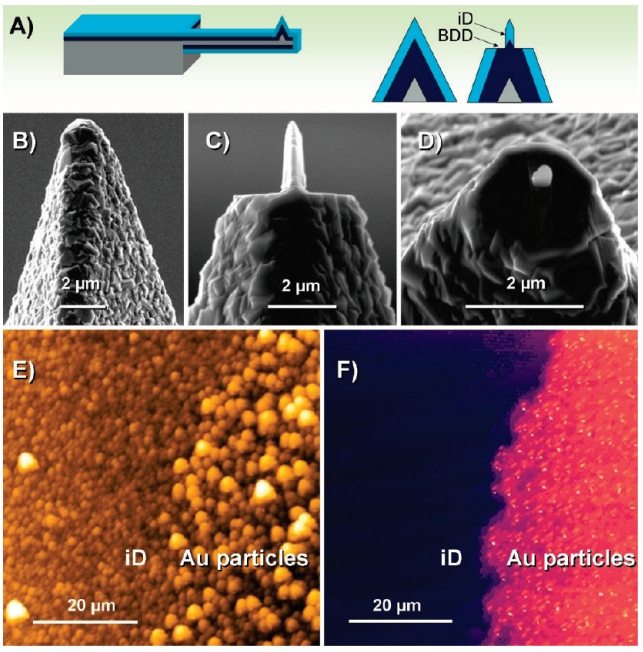

Figure 4. (A) Schematic cross sections of the combined AFM−BDD−SECM probe with conducting and isolating diamond layers. (B) SEM image of Si AFM tip coated with conducting and insulating diamond. (C,D) SEM images of the same tip after FIB milling exposing an electrode (images shown from different angles). (E,F) Combined AFM−SECM measurement. Shown is the topography (E) and the faradaic current (F) of a model substrate. The topographical height and electrochemical current scale are 360 nm and 6 nA, respectively.

sustained for more than 80 scans with only slight degradation in imaging quality (Figure 3C4). The imaging experiment using our nanowire tip was stopped after 83 scans and a total scanned length of 320 000 μm, which were recorded within 18 h in contact mode operation. A video of all 83 scans obtained in contact mode can be found in the Supporting Information.

Combined AFM−SECM Probe. Bifunctional AFM probes with boron-doped diamond (BDD) electrodes recessed from the apex of the AFM tip were obtained by coating commercial silicon cantilevers with a heavily boron-doped and hence highly conductive diamond layer (BDD). In a consecutive step, the coated probes were insulated with intrinsic diamond. Please note that a small part of the AFM chip was covered during the growth of insulating diamond on the boron-doped diamond, leaving a possibility for an electric contact to the tip. Figure 4A shows a schematic of a hybrid silicon/diamond cantilever with multiple diamond layers. A SEM image is shown in Figure 4B. The performance of nano- and microelectrodes for imaging experiments is strongly dependent on the quality of the insulation layer. Exposing the electroactive boron-doped diamond electrode was achieved by focused ion beam (FIB) milling.[16] It was also used to generate sharp diamond tips similar to those produced by self-organized metal masks and ICP etching. This results in a sharp insulating diamond AFM tip and a boron-doped diamond electrode recessed from the tip apex as shown in Figure 4C and D, respectively. The height of the diamond tip and the ring diameter of the exposed ring electrode are dependent on the deposited film thickness of the boron-doped diamond and the FIB milling depth. Typical values for the diamond tip are 1−2 μm and 0.5−1 μm^2 for the electroactive area . This AFM−SECM probe design enables simultaneous recording of AFM and SECM data with no limitation with respect to the investigated samples. The electrode area remains at a fixed and constant distance from the imaged surface during the whole contact-mode measurement given by the height of the sharp diamond tip. Changes of recorded current therefore only depend on the electrochemical nature of the sample. A combined AFM−SECM measurement was recorded at a model sample with insulating and conducting areas to show a proof of principle for measurements with AFM−BDD−SECM electrodes. The images show the topography and the faradaic current in Figure 4E and F, respectively. Obtained images were recorded in contact mode AFM and feedback mode SECM. The imaging experiments were conducted using ferricyanide $Fe(CN)_6^{3-}$, which can be reduced to ferrocyanide $Fe(CN)_6^{4-}$ and subsequently reoxidized to $Fe(CN)_6^{3-}$, by applying a reduction or oxidation potential, E_{Red} = 150 mV or E_{Ox} = 350 mV, respectively. The AFM−BDD−SECM tip was biased at E_{Red} and the model substrate at E_{Ox} to operate in feedback mode.

The analyzed model sample was produced similarly to recently published data.[57] It is boron-doped nanocrystalline diamond that was partially overgrown by insulating diamond. On the left side

of Figure 4E and F, the insulating layer of the imaged sample is completely closed and denoted with iD. On the right side, a gold layer was deposited prior to the overgrowth with insulating diamond. During the overgrowth process, the gold layer melted and formed a discontinuous layer. The insulating diamond grew around these gold islands and formed a partially closed layer with some open conductive areas. These were used as the working electrode when exposed to the liquid for AFM−SECM measurements. When the scanning tip was moved over the conductive areas, ferricyanide was reduced at the AFM tip integrated electrode and subsequently oxidized by the redox active surface, resulting in a cycle of reduction and subsequent oxidation revealing features in the increased current signal which appears as bright spots in Figure 4F. Because the molecule diffusion volumes of the individual conductive areas overlap, the whole area around the conductive parts seems to be more electro-active (brighter in Figure 4F). The completely insulating part of the scanned specimen (left side) leads to a hindered hemispherical diffusion toward the AFM−BDD−SECM tip, resulting in a reduced faradaic current measured at the tip (darker in Figure 4F).

CONCLUSIONS

In summary, an approach for improved AFM probes is shown, which provides enhanced AFM imaging capabilities while it also enables novel AFM−SECM probes with improved electrochemical properties. A fabrication method of a diamond nanowire-based high-resolution AFM probes is presented. Standard silicon cantilevers were overgrown with a conductive and insulating diamond layer. These cantilevers were analyzed for resonance frequency increase and were found to have strongly enhanced quality factors (Q). Self-organizing metal nanomasks were used in a reactive ion etching process (RIE) to generate diamond nanowires with apex radii in the range of 5 nm at the AFM tip apex. The AFM scanning performance of these modified cantilevers was analyzed for investigating the obtainable resolution and the wear characteristics, which revealed significant improvements as compared to commercially available AFM probes. Hybrid AFM−SECM probes were fabricated by integrating a recessed conductive boron-doped diamond electrode at the vicinity of an insulating diamond tip using focused ion beam technology (FIB) fabrication. High-quality boron-doped diamond as electrode material in combination with scanning probe will expand the applicability of combined AFM−SECM measurements based on the exceptional mechanical and electrochemical properties of diamond-based electrodes.

MATERIALS AND METHODS

Diamond Growth. Diamond was grown in an ellipsoidal shaped microwave plasma-enhanced chemical vapor deposition system (MWCVD)[58] at 840 °C, 3 kW microwave power, 3% methane in hydrogen, and pressure of 60 mbar. Diamond was doped by boron by adding 7000 ppm trimethylboron $B(CH_3)_3$ (TMB) to the gas phase. Deposited layers were typically 500 and 350 nm, boron doped and insulating diamond, respectively.

Simulation of Resonance Frequencies. Simulation was performed using the software Ansys for a silicon cantilever with the following dimensions: 225 μm × 35 μm × 7 μm, length, width, and height, respectively. The diamond coating was simulated to range from 0 to 1 μm. Young's moduli were selected as 130 and 950 GPa for silicon and nanocrystalline diamond grown at 3% of methane, respectively.[59] At zero diamond thickness, the simulation gave the same silicon resonance frequency as predicted by eq 1.

Formation of Metal Nanomask. A 20 nm thin gold layer was sputtered on the diamond-coated silicon tips followed by annealing at 1000 °C, which was performed on an inductively heated graphite plate in vacuum for 10 min in a home-build induction furnace.

Etching of Diamond. Etching was carried out using a Sentech ICP SI500 at 5×10^{-2} mbar, 1000 W, and 50 sccm oxygen gas flow for 30 s. During this process, the Au masks were continuously removed, leaving conical formed diamond nanowires.

Characterization. SEM images were taken with a Zeiss 1540 ESB Gemini. Vibrometer measurements were performed with a Polytec scanning laser doppler vibrometer. AFM imaging was performed with a Veeco Multimode Nanoscope V probe microscope (CA). For electrochemical measurements, the AFM liquid cell was equipped with an Ag/AgCl reference electrode and Pt counter electrode. Potentials were applied using a BioLogic VMP3 multichannel potentiostat. The recorded electrochemical signal was fed into the AFM system using the analog signal input. 0.2 M $K_3[Fe(CN)_6]$ was used as redox mediator.

Wear and Resolution Characterization. Resolution scans were done by imaging λ-phage single-strand DNA on mica. The tip apex radius was determined by calculating $r = (w - 1)/2$, where w is the FWHM of a line scan perpendicular to a DNA filament, which was measured to have a height of 1 nm. Contact mode AFM was performed on a planar NCD sample of 1 × 1 cm^2. The imaging parameters for each scan were 384 lines, 5 × 5 μm at a speed of 5 $\mu m\ s^{-1}$. The sharpened diamond tip scanned 83 images considering trace and retrace scan of the tip, resulting in a total scan distance of 320 000 μm. Commercial probes were Si tapping mode probes from Nanosensors with a resonance frequency of ca. 150 kHz and a nominal force constant of approximately 50 $N\ m^{-1}$. The dimensions of the cantilever were 225, 35, and 7 μm in length, width, and height, respectively. Diamond-coated contact mode probes were obtained from Nanosensors and had a resonance frequency of 15 kHz and a nominal force constant of 0.5 $N\ m^{-1}$. The dimensions of the cantilever were 450, 50, and 2 μm in length, width, and height, respectively.

ASSOCIATED CONTENT

Supporting Information. Real-time vibrational characterization of cantilevers using a vibrometer setup. Two videos showing first and second harmonics oscillations. Fast motion video of 83 contact mode AFM scans with diamond-coated and sharpened tip on NCD surface. This material is available free of charge via the Internet at http://pubs.acs.org.

AUTHOR INFORMATION

Corresponding Author

*Phone: +(0)49-0761-5159-283. E-mail: waldemarsmirnov@gmx.de.

Present Addresses

[||]Cardiff School of Physics and Astronomy, Queens Buildings, The Parade, Cardiff CF24 3AA, United Kingdom.

■ ACKNOWLEDGMENT

This work was supported by the Baden-Württemberg Stiftung "Einzelmolekulare Strukturanalyse und zelluläre Transportmechanismen an Poren-formenden Peptiden" (P-LS-SPII/23).

C.K. acknowledges the Focused Ion Beam Center UULM, which is supported by FEI Company (Eindhoven, Netherlands), the German Science Foundation (INST40/385-F1UG), and the Struktur- und Innovationsfonds Baden-Württemberg.

■ REFERENCES

(1) Foubert, P.; Vanoppen, P.; Martin, M.; Gensch, T.; Hofkens, J.; Helser, A.; Seeger, A.; Taylor, R. M.; Rowan, A. E.; Nolte, R. J. M.; De Schryver, F. C. *Nanotechnology* **2000**, *11*, 16–23.

(2) Proksch, R.; Lal, R.; Hansma, P. K.; Morse, D.; Stucky, G. *Biophys. J.* **1996**, *71*, 2155–2157.

(3) Korchev, Y. E.; Raval, M.; Lab, M. J.; Gorelik, J.; Edwards, C. R. W.; Rayment, T.; Klenerman, D. *Biophys. J.* **2000**, *78*, 2675–2679.

(4) Bard, A. J.; Fan, F. R. F.; Kwak, J.; Lev, O. *Anal. Chem.* **1989**, *61*, 132–138.

(5) Bard, A. J.; Fan, F.-R. F.; Pierce, D. T.; Unwin, P. R.; Wipf, D. O.; Zhou, F. *Science* **1991**, *254*, 68–74.

(6) Liu, B.; Rotenberg, S. A.; Mirkin, M. V. *Proc. Natl. Acad. Sci. U.S. A.* **2000**, *97*, 9855–9860.

(7) Bai, S.-J.; Fabian, T.; Prinz, F. B.; Fasching, R. J. *Sens. Actuators, B* **2008**, *130*, 249–257.

(8) Holt, K. B.; Hu, J.; Foord, J. S. *Anal. Chem.* **2007**, *79*, 2556–2561.

(9) Casero, E.; Vazquez, L.; Parra-Alfambra, A. M.; Lorenzo, E. *Analyst* **2010**, *135*, 1878–1903.

(10) Allison, D. P.; Mortensen, N. P.; Sullivan, C. J.; Doktycz, M. J. *Wiley Interdiscip. Rev.: Nanomed. Nanobiotechnol.* **2010**, *2*, 618–634.

(11) Anne, A.; Cambril, E.; Chovin, A.; Demaille, C. *Anal. Chem.* **2010**, *82*, 6353–6362.

(12) Wolfschmidt, H.; Baier, C.; Gsell, S.; Fischer, M.; Schreck, M.; Stimming, U. *Materials* **2010**, *3*, 4196–4213.

(13) Bertoncello, P. *J. Energy Environ. Sci. (RSC)* **2010**, *3*, 1620–1633.

(14) Macpherson, J. V.; Unwin, P. R. *Anal. Chem.* **2000**, *72*, 276–285.

(15) Shin, H.; Hesketh, P. J.; Mizaikoffff, B.; Kranz, C. *Sens. Actuators, B* **2008**, *134*, 488–495.

(16) Kranz, C.; Friedbacher, G.; Mizaikoff, B. *Anal. Chem.* **2001**, *73*, 2491–2500.

(17) Kranz, C.; Kueng, A.; Lugstein, A.; Bertagnolli, E.; Mizaikoff, B. *Ultramicroscopy* **2004**, *100*, 127–134.

(18) Kranz, C.; Wiedemair, J. *Anal. Bioanal. Chem.* **2008**, *390*, 239–243.

(19) Macpherson, J. V.; Unwin, P. R. *Anal. Chem.* **2001**, *73*, 550–557.

(20) Dobson, P. S.; Weaver, J. M. R.; Holder, M. N.; Unwin, P. R.; Macpherson, J. V. *Anal. Chem.* **2004**, *77*, 424–434.

(21) Gullo, M. R.; Frederix, P. L. T. M.; Akiyama, T.; Engel, A.; deRooij, N. F.; Staufer, U. *Anal. Chem.* **2006**, *78*, 5436–5442.

(22) Avdic, A.; Lugstein, A.; Wu, M.; Gollas, B.; Pobelov, I.; Wandlowski, T.; Leonhardt, K.; Denuault, G.; Bertagnolli, E. *Nanotechnology* **2011**, *22*, 145306.

(23) Kueng, A.; Kranz, C.; Lugstein, A.; Bertagnolli, E.; Mizaikoff, B. *Angew. Chem., Int. Ed.* **2003**, *42*, 3238–3240.

(24) Shin, H.; Hesketh, P. J.; Mizaikoff, B.; Kranz, C. *Anal. Chem.* **2007**, *79*, 4769–4777.

(25) Pires, D.; Hedrick, J. L.; De Silva, A.; Frommer, J.; Gotsmann, B.; Wolf, H.; Despont, M.; Duerig, U.; Knoll, A. W. *Science* **2010**, *328*, 732–735.

(26) Szoszkiewicz, R.; Okada, T.; Jones, S. C.; Li, T.-D.; King, W. P.; Marder, S. R.; Riedo, E. *Nano Lett.* **2007**, *7*, 1064–1069.

(27) Snow, E. S.; Campbell, P. M. *Appl. Phys. Lett.* **1994**, *64*, 1932–1934.

(28) Piner, R. D.; Zhu, J.; Xu, F.; Hong, S.; Mirkin, C. A. *Science* **1999**, *283*, 661–663.

(29) Kim, K. H.; Sanedrin, R. G.; Ho, A. M.; Lee, S. W.; Moldovan, N.; Mirkin, C. A.; Espinosa, H. D. *Adv. Mater.* **2008**, *20*, 330–334.

(30) Cen, C.; Thiel, S.; Mannhart, J.; Levy, J. *Science* **2009**, *323*, 1026–1030.

(31) Vettiger, P.; Cross, G.; Despont, M.; Drechsler, U.; Durig, U.; Gotsmann, B.; Haberle, W.; Lantz, M. A.; Rothuizen, H. E.; Stutz, R.; Binnig, G. K. *IEEE Trans. Nanotechnol.* **2002**, *1*, 39–55.

(32) Kado, H.; Yokoyama, K.; Tohda, T. *Rev. Sci. Instrum.* **1992**, *63*, 3330–3332.

(33) Dai, H. J.; Hafner, J. H.; Rinzler, A. G.; Colbert, D. T.; Smalley, R. E. *Nature* **1996**, *384*, 147–150.

(34) Janchen, G.; Hoffmann, P.; Kriele, A.; Lorenz, H.; Kulik, A. J.; Dietler, G. *Appl. Phys. Lett.* **2002**, *80*, 4623–4625.

(35) Cheung, C. L.; Hafner, J. H.; Odom, T. W.; Kim, K.; Lieber, C. M. *Appl. Phys. Lett.* **2000**, *76*, 3136–3138.

(36) Spear, K. E.; Dismukes, J. P. *Synthetic Diamond: Emerging CVD Science and Technology*; Wiley: New York, 1994.

(37) Nebel, C. E.; Rezek, B.; Shin, D.; Uetsuka, H.; Yang, N. *J. Phys. D: Appl. Phys.* **2007**, *40*, 6443–6466.

(38) Walsh, D. A.; Lovelock, K. R. J.; Licence, P. *Chem. Soc. Rev.* **2010**, *39*, 4185–4194.

(39) Niedermann, P.; Hanni, W.; Blanc, N.; Christoph, R.; Burger, J. *J. Vac. Sci. Technol., A* **1996**, *14*, 1233–1236.

(40) Tanasa, G.; Kurnosikov, O.; Flipse, C. F. J.; Buijnsters, J. G.; van Enckevort, W. J. P. *J. Appl. Phys.* **2003**, *94*, 1699–1704.

(41) Malave, A.; Oesterschulze, E.; Kulisch, W.; Trenkler, T.; Hantschel, T.; Vandervorst, W. *Diamond Relat. Mater.* **1999**, *8*, 283–287.

(42) Shibata, T.; Kitamoto, Y.; Unno, K.; Makino, E. *J. Microelectromech. Syst.* **2000**, *9*, 47–51.

(43) Unno, K.; Shibata, T.; Makino, E. *Sens. Actuators, A* **2001**, *88*, 247–255.

(44) Unno, K.; Kitamoto, Y.; Shibata, T.; Makino, E. *Smart Mater. Struct.* **2001**, *10*, 730–735.

(45) Kim, K. H.; Moldovan, N.; Ke, C. H.; Espinosa, H. D.; Xiao, X. C.; Carlisle, J. A.; Auciello, O. *Small* **2005**, *1*, 866–874.

(46) Agrawal, R.; Moldovan, N.; Espinosa, H. D. *J. Appl. Phys.* **2009**, *106*, 064311–064316.

(47) Liu, J.; Grierson, D. S.; Moldovan, N.; Notbohm, J.; Li, S.; Jaroenapibal, P.; O'Connor, S. D.; Sumant, A. V.; Neelakantan, N.; Carlisle, J. A.; Turner, K. T.; Carpick, R. W. *Small* **2010**, *6*, 1140–1149.

(48) Chung, K.-H.; Kim, D.-E. *Ultramicroscopy* **2007**, *108*, 1–10.

(49) Smirnov, W.; Kriele, A.; Yang, N.; Nebel, C. E. *Diamond Relat. Mater.* **2010**, *19*, 186–189.

(50) Williams, O. A.; Douheret, O.; Daenen, M.; Haenen, K.; Osawa, E.; Takahashi, M. *Chem. Phys. Lett.* **2007**, *445*, 255–258.

(51) Williams, O. A.; Hees, J.; Dieker, C.; Jager, W.; Kirste, L.; Nebel, C. E. *ACS Nano* **2010**, *4*, 4824–4830.

(52) Ahmad, R. K.; Parada, A. C.; Hudziak, S.; Chaudhary, A.; Jackman, R. B. *Appl. Phys. Lett.* **2010**, *97*, 093103–093103.

(53) Buffat, P.; Borel, J. P. *Phys. Rev. A* **1976**, *13*, 2287.

(54) Tan, B. J. Y.; Sow, C. H.; Koh, T. S.; Chin, K. C.; Wee, A. T. S.; Ong, C. K. *J. Phys. Chem. B* **2005**, *109*, 11100–11109.

(55) Wong, E. W.; Sheehan, P. E.; Lieber, C. M. *Science* **1997**, *277*, 1971–1975.

(56) Zhu, Y.; Inada, H.; Nakamura, K.; Wall, J. *Nat. Mater.* **2009**, *8*, 808–812.

(57) Hees, J.; Hoffmann, R.; Kriele, A.; Smirnov, W.; Obloh, H.; Glorer, K.; Raynor, B.; Driad, R.; Yang, N.; Williams, O. A.; Nebel, C. E. *ACS Nano* **2011**, *5*, 3339−3346.

(58) Füner, M.; Wild, C.; Koidl, P. *Appl. Phys. Lett.* **1998**, *72*, 1149–1151.

(59) Kriele, A.; Williams, O. A.; Wolfer, M.; Brink, D.; Muller-Sebert, W.; Nebel, C. E. *Appl. Phys. Lett.* **2009**, *95*, 031905.